Collisions of noble gases with supercooled sulfuric acid–water solutions

Peter Behr, Ulrich Scharfenort and Reinhard Zellner

Received 4th December 2008, Accepted 13th May 2009
First published as an Advance Article on the web 11th June 2009
DOI: 10.1039/b821751c

The collisions of hyperthermal noble gases (He, Ne, Ar, Kr, Xe) with supercooled binary sulfuric acid–water mixtures (57–77 wt%) were explored in the temperature range between 210 and 240 K. The experiments were performed by directing a molecular beam of the respective gases onto a continuously renewed liquid surface and monitoring the velocity of the scattered molecules by mass spectrometry. Depending on the initial translational energies and molecular masses, we observe both inelastic scattering from the surface as well as thermalization followed by subsequent desorption. The experiments indicate that the repulsive momentum transfer in the inelastic scattering channel increases with increasing mass of the impinging gas, while it is only weakly affected by the initial velocities. The final energy of the thermally desorbing atoms can always be approximated by a Maxwell–Boltzmann distribution equal to the liquid bulk phase temperature. The influence of the binary composition of the liquid phase is only noticeable in the case of Ne, whilst this dependence diminishes for gases with molecular masses ≥ 40 amu. The probability of thermalisation relative to inelastic scattering increases with the bulk phase temperature, independent of the molecular masses of the colliding gas. In contrast, the fractional energy transfer during collision does not increase with temperature, except for Neon. These results can be interpreted in the model framework of hard-sphere collisions of noble gases with the surface, during which water and sulfuric acid molecules interact independently with the impinging gas.

1. Introduction

The initial step of the uptake of a translationally hot gas phase molecule into a liquid phase is the collision of this molecule with the molecules at the outer surface of the condensed phase. During this step the gas molecules may be scattered inelastically or else transfer excess translational energy onto the surface molecules and eventually thermalise in the interfacial layer. Driven by the thermal motions of the surface molecules, the thermalised molecules may subsequently desorb and return into the gas phase or else may be transported into the bulk *via* the interfacial region.

On a microscopic scale various parameters affect the trajectories of the impinging gas. The structure and composition of the liquid surface as well as the nature of the colliding gas molecule determine the range of repulsive and attractive interactions including the collision energy, the position and direction of impact on the surface as well as the orientations and internal motions of the gas and liquid molecules. A gas molecule striking the surface encounters various impact sites that are composed of surface molecules which continuously adopt new configurations during reorientation and diffusion in a fluid interface. Hence, the intermolecular energy transfer varies widely over theses surface sites. The instantaneous local contours and compositions of the surface govern the momentum transfer, the recoil direction per collision and the extent of multiple collisions.[1–5]

Institute of Physical and Theoretical Chemistry, University of Duisburg-Essen, D-45117 Essen, Germany

The study of the interaction dynamics of gases with a fluid interface on a molecular scale raises several questions:

- How do microscopic morphologies influence the gas–liquid energy transfer?
- Are liquid surfaces sufficiently disordered to allow incoming atoms to collectively sample most surface sites regardless of their approach direction?
- Is the collision dynamics affected by bulk phase parameters such as composition, density, surface tension, bulk compressibility or viscosity?
- What effect on gas–liquid repulsive interaction and surface accommodation is exhibited by the temperature of the surface?

These questions can be addressed by molecular beam techniques as conventionally employed to the study of gas–gas and gas–solid collisions. The adoption of this technique to gas–liquid interactions has been pioneered by Nathanson *et al.*[1–3,6] using molten metals[7–9] and fluids with low vapour pressure. Their experiments have presented considerable support for the fundamental collision paradigm that gas molecules scatter from a liquid surface *via* two distinct channels: trapping–desorption (TD) and inelastic scattering (IS). While the TD channel consists of gas molecules that desorb from the surface with a Maxwell–Boltzmann translational energy distribution consistent with the surface temperature, the IS channel population typically escapes the surface with a much higher fraction of its incident energy. Similar methods have been used by Minton and co-workers[10] to investigate reactive and inelastic scattering from liquid hydrocarbon surfaces. These authors used velocity and angle resolved mass spectrometry to study the reactions of Cl, O,

and O_2 with liquid squalane at 5–125 kcal mol^{-1} collision energies.[10] Studies with self-assembled monolayers (SAMs) of alkanethiols have equally produced evidence for "two-channel" (TD/IS) dynamics when sampled for a variety of surface conditions, chain lengths and types of incident gas molecules.[11]

The first quantum state resolved scattering study was performed by McCaffery and co-workers.[12] These authors explored aspects of gas–liquid interactions by measurements of internal state populations of cold I_2 gas molecules impinging on liquid gallium and polysiloxane oil using laser induced fluorescence (LIF). State-resolved LIF measurements of OH formed by reaction of O atoms with liquid surfaces have been performed by McKendrick and co-workers.[13] The vibrational product excitation was found to be fairly modest and to increase slightly as the surface temperature was increased.[13] Nesbitt and co-workers have developed high resolution IR absorption methods to probe inelastic scattering of CO_2 from a series of perfluorinated hydrocarbons and hydrogen bonded liquids.[14]

In addition to the various experimental approaches, the scattering of gas molecules on liquid surfaces has also become the subject of theoretical studies. Hase and co-workers introduced methods to describe surface structures of self-assembled monolayers (SAM) using molecular mechanics (MM)[15] to describe the motion of the surface, while for the scattering of species accurate quantum mechanical (QM)[16] potentials have been utilized. Kim and Schatz[17] extended this approach to the molecular motion at the interface of liquids in order to predict the reactive scattering dynamics of impinging O atoms.

With this background a more sophisticated picture for the scattering dynamics at the gas–liquid interface has begun to develop. While trapping desorption (TD) remains to be characterized by a Boltzmann velocity, it is additionally found that the rotational state distributions also matches the liquid temperature. Moreover, in impulsive/direct reactive scattering (DRS) recoiling molecules retain a large fraction of their incident rotational and translational energy. The calculations also indicate that molecular vibrations, on the contrary, are mostly decoupled from the surface temperature in either TD or DRS scattering channels. This indicates incomplete equilibration and suggests an upper limit for surface interaction in the range of 10–100 ps for intermolecular vibrational energy transfer.

In the present study we have investigated the interactions of noble gases with liquid binary sulfuric acid–water surfaces. The focus of our work is on the mass effects of the collision kinematics as well as its dependence on the composition of the liquid and its temperature. Moreover, since we are dealing with noble gases, effects such as internal excitations of impinging or recoiling species or reactive contributions to the scattering channels can be neglected.

The choice in our experiment of supercooled sulfuric acid solutions is motivated by the role of sulfuric acid particles in heterogeneous reactions in the stratosphere leading to ozone depletion.[18,19] Although it is realized that encounters between noble gases and sulfuric acid surfaces are not atmospherically relevant it is still expected that some of the important physical aspects of the gas–liquid interactive behaviour of sulfuric acid–water surfaces are more easily identified when chemical aspects are excluded. The corresponding results for the interaction of HCl with such surfaces, which is indeed atmospherically relevant, will be reported in a forthcoming publication.[20]

The initial interaction between a gas phase molecule and the H_2SO_4–H_2O surface depends on the composition and structure of the interfacial region of the acid. Sum frequency generation (SFG) studies of such surfaces indicate that the surface water composition of liquid sulfuric acid solutions varies as a function of the binary composition of the bulk[21,22] but is not affected by temperature between 273 K and 216 K.[23] In particular, species from below the surface of 38 wt% solutions tend to orient water molecules at the surface. The surface for 58 wt% solutions, however, features H_2SO_4–H_2O complexes both at 273 K and supercooled at 216 K. In addition, Auger electron spectroscopy[24] of H_2SO_4 solutions indicates that there is little segregation of the lower surface H_2SO_4 to the surface, implying that the interfacial composition should be close to the H_2SO_4–H_2O ratio in the bulk. Raman measurements show that binary H_2SO_4–H_2O mixtures in the investigated concentration range at 298 K are extensively ionised, with little or no molecular H_2SO_4 present.[25,26] This is also supported by thermodynamic calculations which predict an almost complete dissociation of H_2SO_4 in the temperature range between 213 K and 243 K.[27]

An important additional aspect of the change in relative composition of the fluid and of temperature with respect to collision dynamics is that of viscosity. The viscosity of H_2SO_4–H_2O solutions increases by almost two orders of magnitude in the concentration range from 57 wt% to 77 wt% at 213 K and decreases by more than one order of magnitude in the temperature interval from 213 K to 243 K.[28] This variation in the bulk phase viscosity raises the question whether or not the collision of the impinging gas is affected by an elastic response of the fluid interface as determined by parameters of the condensed phase *i.e.* the viscosity.

Experimental

The experiments were conducted by application of a molecular beam scattering technique similar to the one developed by Nathanson and coworkers.[1,3] A schematic representation of

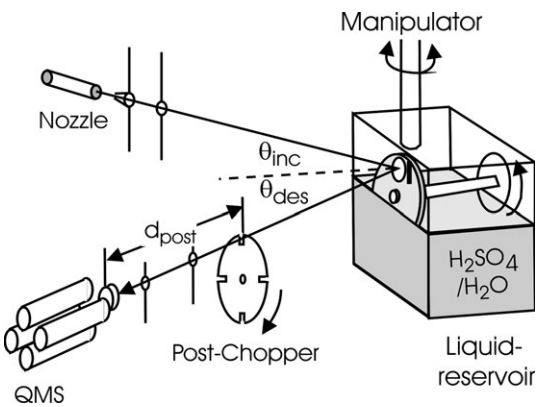

Fig. 1 Schematic representation of experimental set-up.

the experimental set-up is shown in Fig. 1. In this experiment continuous molecular beams are created by expanding a gas mixture at 1.0–1.2 bar through an aperture of $\sim$0.1 mm in diameter. After passing through a 1 mm diameter conical skimmer the beam is collimated by a 2 mm diameter hole in the main chamber with an angular divergence of $<1^\circ$. At an incident angle $\theta_{inc} = 45^\circ$ the beam strikes a 2.9×4.1 mm^2 area of the vertically oriented liquid surface. The initial translational energy, as obtained by adiabatic expansion of a gas mixture into vacuum, is controlled by several factors including the geometry of the nozzle and the skimmer, the relative concentration of the seeding gas and the temperature of the nozzle. The expansion of pure noble gases without intermolecular interactions generates initial translation energies of almost $(5/2)RT$ ($\sim$6 kJ mol^{-1} at 298 K). Hyperthermal translational energies of around 140 kJ mol^{-1} with a variance of approximately $\pm$ 20 kJ mol^{-1} were achieved by seeding the noble gases with H_2 and by varying the nozzle temperature. The experimentally obtained translational energy for Ne, however, was only 85 kJ mol^{-1} due to the difficulties in achieving higher translational energies by seeding light-weight gases in H_2.

The initial translational energies of the incident beams were determined in a linear alignment of the five vacuum chambers by directly measuring the flight-time of the pulsed molecular beam over a certain distance from the post-chopper to the ionisation field of the QMS. Because of the finite opening time of the chopper wheel, the velocity distribution is somewhat perturbed by this effect and was extracted from the measured time-of-flight signal by a corresponding deconvolution procedure. The accuracy of our energy measurement is estimated to be $\pm$5 kJ mol^{-1}.

Continuously renewed liquid films of H_2SO_4–H_2O were generated by partially immersing a vertically rotating wheel in the acid. This techniques was first developed by Lednovich and Fenn[29] and subsequently improved by Nathanson *et al.*[4,30] The reservoir drawn in Fig. 1 shows a 4.5 cm in diameter gold-coated brass wheel partially submersed in the liquid. As the wheel rotates it is coated with a thin fresh liquid film. In order to ensure uniform rotation the wheel is driven by a stepper motor (Phytron, VSS 52 200.5), especially designed for use in ultra-high vacuum. The molecular beam interacts with the liquid surface through a 3 mm in diameter hole located in front of the wheel. The reservoir is otherwise sealed to suppress evaporation of the liquid into the scattering chamber. To reduce corrosion against sulfuric acid the cubic Ti box ($72 \times 72 \times 72$ mm) is completely covered inside with Teflon with a wall thickness of $\sim$5 mm.

The liquid reservoir is suspended from a post which can be rotated in order to vary the incident angle of the molecular beam. Using a laser beam, the gold coated wheel acts as a reflecting surface which enables the adjustment of the nozzle and the QMS-ionisation field in plane with the surface normal of the wheel. Laser reflections from the rotating wheel are sharp and deviate by less than $\pm1^\circ$, indicating that the surface is macroscopically flat and that the wheel does not wobble strongly during its rotation.

The rotation speed of the wheel was varied between 0.025 and 0.25 Hz without any indication of a change in the experimental results. At 0.25 Hz rotation speed the residence time of the liquid film on the wheel between mixing in the reservoir is 2 s, the exposure time to the molecular beam at $\theta_{inc} = 45^\circ$ is about 0.1 s. These times imply that the free surfaces should not be contaminated by ambient gases during exposure since the dominant residual gases at 10^{-6}–10^{-7} mbar do not stick. The reservoir is filled with 15 ml of a degassed sulfuric acid–water mixture. It is cooled by circulating a cold methanol–ethanol mixture through Teflon coated cooling tubes that pass through the liquid. During cooling of the reservoir the scattering chamber is gradually evacuated by a 1600 l s^{-1} oil free turbo-molecular pump (TMP 1600 MC). The experiments were performed with sulfuric acid concentrations ranging from $\sim$57 to 77 wt% for which the acid is still liquid and the results are not significantly affected by the collisions of the impinging gas with desorbing water molecules. From direct measurements of the desorbing flux of water molecules as a function of the water content of the binary solution we estimate that the change of the composition as a result of water evaporation during the time scale of the experiment is $<$0.2 wt%.

The atoms that scatter or desorb from the liquid interface are detected by a doubly differentially pumped mass spectrometer with cross beam ionisation (QMG 422, Balzers (Pfeiffer-Vacuum)) oriented at a fixed angle of 90° to the incident beam. This fixed geometry allows scattered signals to be detected only at $\theta_{fin} = 90^\circ - \theta_{inc}$. The cross beam ioniser is positioned 38.0 ± 0.3 cm from the liquid surface and views a 2.9×4.1 mm section of the surface at $\theta_{inc} = 45^\circ$ through two collimating apertures. The flight times of the scattered or desorbing species are determined by chopping the flux of the recoiling atoms into short pulses with a 10 cm in diameter spinning wheel with two 4 mm slots. This method generates 67 μs pulses with the wheel spinning at 200 Hz. The arrival times of the products are then measured at the MS ioniser which is positioned 28.0 ± 0.2 cm away from the chopper. The TOF spectra are recorded by a multichannel scaler (Fast, P7882-2) in 0.25 μs bins.

The TOF spectra have been corrected for all electronic offsets and the ion flight time from the ionizer to the detector, $t_{i,d}$, which is given by

$$t_{i,d} = d_{i,d}\sqrt{m_g}/\sqrt{2E}$$

where $d_{i,d}$ is the distance from ionizer to detector, m_g is the mass of the species and E is the translational energy. The calibration of the additional time offsets for all noble gases from He to Xe indicate a linear dependence of $t_{i,d}$ with $\sqrt{m_g}$ and $1/\sqrt{2E}$ for field axis voltages ranging from 18 eV to 60 eV. At a typical acceleration voltage of 48 eV the additional flight time, $t_{i,d}$, was given for each mass by $t_{i,d} = 5.7\ \sqrt{[m_g(\text{amu})]}$.

It has to be pointed out that in the post-chopper configuration the chopper wheel in Fig. 1 is positioned between the surface and the mass spectrometer. Hence we measure velocity distributions of the recoiling molecules and not the residence times of the gas on or in the liquid.

3. Data analysis and interpretation

In the following we discuss typical observations and their information content.

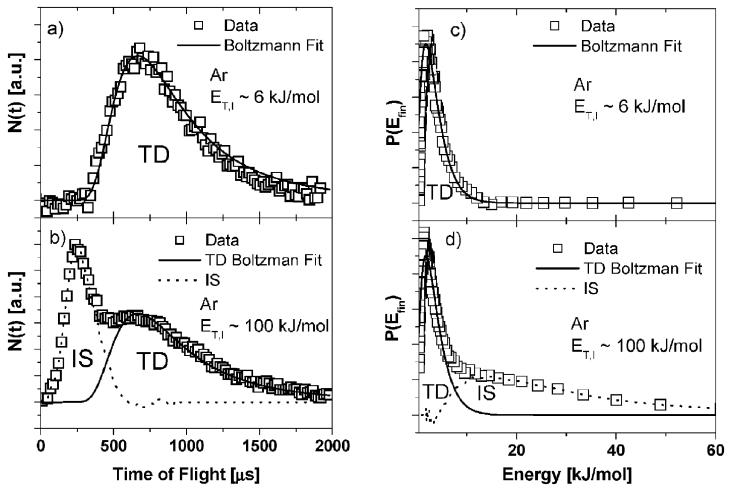

Fig. 2 (a) and (b): Observed intensity profiles of backscattered Ar atoms from a sulfuric acid–water surface at $T = 213$ K and 73 wt%. The curves shown in (a) and (b) are for initial impact energies of 6 and 100 kJ mol^{-1}. The squares are experimental points and the solid and dashed curves are calculated from the corresponding $P(E_{fin})$ distributions in (c) and (d): For an explanation of thermal desorption (TD) and inelastic scattering (IS) see text. (c) and (d): Translational energy distribution of backscattered Ar atoms from a sulfuric acid–water surface at $T = 213$ K and 73 wt%. The data points are derived from the TOF spectra in Fig. 2a–b. The areas under the solid and dashed curves are the estimated contributions of the TD and IS channels.

Fig. 2a and b show TOF-spectra for the scattering of Ar atoms with two different initial translational energies, E_{inc}, of 6 kJ mol^{-1} (a) and 100 kJ mol^{-1} (b), respectively, from a surface of a 73 wt% sulfuric acid–water solution at 213 K. Incident and scattering angles are 45° each and in plane with respect to the surface normal. The measured MS signals are proportional to the number densities $N(t)$ and are plotted *versus* the arrival time t for the molecules to traverse the distance d_{post}. The spectra are corrected for electronic and timing offsets and used to compute the relative fluxes or intensities, $I(E_{fin})$, of the scattered atoms from the relations

$$I(E_{fin}) = CN(t)t^2 \text{ and } E_{fin} = 1/2m_g\,(L/t)^2$$

where C is a normalisation constant and L is the flight path (28 cm). The calculated intensities $I(E_{fin})$ are proportional to the relative probabilities, $P(E_{fin})$, that the atoms will scatter from the liquid surface at final energy E_{fin}. The corresponding relative probabilities, $P(E_{fin})$, *versus* the final energies E_{fin} are plotted in Fig. 2c and d. As can be seen the energy distributions behave like mirror images of the TOF spectra because of the inverse relationship between flight-time and recoil energy. The component that is narrow and low in energy maps into the broad and slow component in time.

The energy analysis of the TOF spectra has been made by direct inversion without deconvolution with the 67 μs opening time of the chopper wheel. This inversion itself is uncertain to within ±3% in $P(E_{fin})$ and ±2 kJ mol^{-1} in E_{fin}, whereas the errors in the flight path of ±0.1 cm and in the arrival time of ±1 μs typically generate total errors in the calculated energies of ±1 kJ mol^{-1}. The difference $\Delta E = E_{inc} - E_{fin}$ is the translational energy of the impinging atoms lost to the liquid phase molecules.

As can be seen from Fig. 2 the energy release to the surface is different for different initial translational energies of the impinging atoms. Whereas the TOF- and energy spectra of recoiled atoms which strike with $E_{inc} = 6$ kJ mol^{-1} are single peaked (Fig. 2a and c) the corresponding spectra for atoms with $E_{inc} = 100$ kJ mol^{-1} (Fig. 2b and d) are bimodal, consisting of a fast and narrow peak which is superimposed onto a slower and broader peak. We attribute this bimodality to two limiting processes which often occur in gas–solid[31–33] and gas–liquid collisions[4,30,34] namely trapping–desorption (TD) and inelastic scattering (IS).

The solid lines in Fig. 2a–d correspond to a Maxwell–Boltzmann distribution calculated for the prevailing temperature of the liquid bulk ($T_{liq.} = 213$ K). In calculating this distribution we assume that there is no temperature gradient between the bulk phase and the surface and that the desorbing molecules are in contact with the liquid surface long enough to undergo statistical energy exchange and thermal equilibration. Since the assignments of the observed peaks are based on measured translational energies only and not on residence times, the "thermal desorption" channel includes molecules which temporarily dissolve into the bulk and then desorb as well as those which accommodate on the surface through multiple collisions and depart at thermal velocities.

Within this two channel model, the overall scattering probability $P(E_{fin})$ is the sum of the TD and IS components with the relative weighting of the two fractions according to the relation:

$$P(E_{fin}) = \alpha_{th}\,P_{TD}\,(E_{fin}) + (1 - \alpha_{th})\,P_{IS}\,(E_{fin}) \qquad (1)$$

where $P_{TD}(E_{fin})$ is set equal to a Boltzmann distribution at T_{liq};

$$P_{TD}(E_{fin}) = (RT_{liq})^{-2}\,E_{fin}\exp(-E_{fin}/RT_{liq}) \qquad (2)$$

In here, α_{th} is the fraction of molecules which leave the liquid surface at $\theta_{fin} = 90° - \theta_{inc}$ *via* the TD channel. To estimate α_{th} as well as $P_{IS}(E_{fin})$, we fit a Boltzmann distribution $P_{TD}\,(E_{fin})$ to the overall $P(E_{fin})$ curve such that the peak of $P_{TD}(E_{fin})$ at RT_{liq} matches the value of the measured $P(E_{fin})$ at the same energy. This procedure assumes that at recoil energies of $RT_{liq.}$

and lower, all of the signal is due to molecules desorbing thermally from the liquid. The trapping–desorption contribution is then subtracted from the overall curve to yield the inelastic scattering contribution $P_{IS}(E_{fin})$.

The methods described here were adapted from Nathanson *et al.*[3] The fitting procedures used in this work differ by using an unconstrained form for $P_{IS}(E_{fin})$ instead of an analytical form as used by Hurst *et al.*[33] and Rettner and co-workers.[31] Nevertheless, a direct comparison shows[3] that the values of α_{th} and $(\Delta E_{IS})/E_{inc}$ were very similar.

4. Results

In our investigations we have studied the impact of various parameters such as initial translational energy of the atoms, atomic mass, relative surface composition and surface temperature on the scattering behaviour of noble gas atoms from sulfuric acid surfaces. In addition, we have also investigated the dependence of the scattering behaviour on the angle of incidence. The effects found, however, were very small and will be presented in a forthcoming publication.[20]

In Fig. 3a and 4a we present the fractional energy releases, $\Delta E_{IS}/E_{inc}$, of the inelastic scattered species (IS), whereas Fig. 3b and 4b display the ratio of the integrated areas for the trapping–desorption peaks, I_{TD}, divided by the total integration areas $I_{Total} = I_{IS} + I_{TD}$. To enable a direct comparison between the impulsive momentum transfer and the relative fluxes of the recoiled and the thermal desorbing species, the same abscissa are used in Fig. 3a/b and Fig. 4a/b for the different surface temperatures and binary compositions, respectively. It must be emphasized that the observed energy transfer, $\Delta E_{IS}/E_{inc}$, is only due to those molecules which scatter inelastically from the surface. Therefore, the IS component represents only a fraction of the total energy

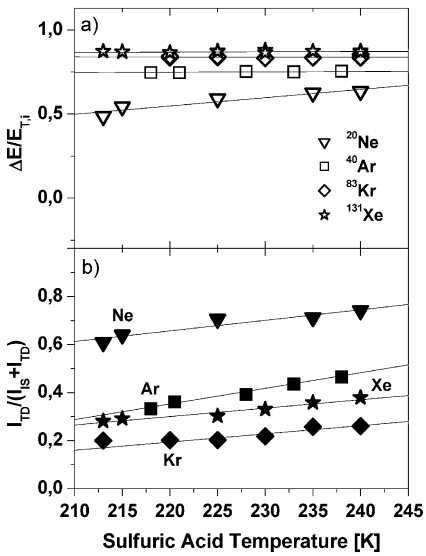

Fig. 3 (a) and (b): Relative energy release, $\Delta E_{IS}/E_{inc}$ (open symbols) and integrated signal intensities, $I_{TD}/(I_{IS} + I_{TD})$ (filled symbols), in collisions of noble atoms with sulfuric acid surfaces (~70 wt%) for different temperatures of the surface films. Angle of incidence = 45°. The different gases are indicated by different symbols; their masses are given by superscripts.

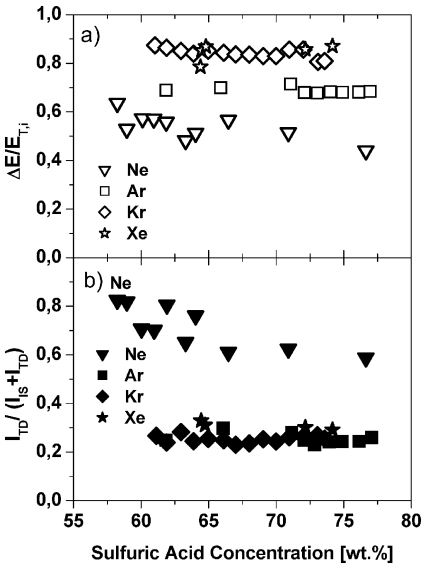

Fig. 4 (a) and (b): Relative energy release, $\Delta E_{IS}/E_{inc}$ (open symbols) and integrated signal intensities, $I_{TD}/(I_{IS} + I_{TD})$ (filled symbols), as a function of the composition of the liquid phase. Temperature 213 K; angle of incidence = 45°. The different gases are indicated by different symbols.

released to the surface molecules. The translational energy lost by the recoiled species does not include the fraction which is dissipated by molecules that transfer their total translation energy to the surface molecules before desorbing with a thermal distribution.

The temperature dependence of the energy release of scattered noble gases (Ne, Ar, Kr, Xe) from the sulfuric acid surface are shown in Fig. 3a. In this Figure we present the fractional energy release relative to the initial translational energy, $\Delta E_{IS}/E_{inc}$, as calculated from the measured difference between the initial translational energy and the average translational energy of the recoiled species, $(E_{inc} - E_{IS})/E_{inc}$. The integrated signal intensities for thermally desorbing species, I_{TD}, relative to the sum of the integrated signal intensities, $I_{IS} + I_{TD}$, are displayed in Fig. 3b. In each case the results are plotted against the temperature of the liquid between 213 K and 243 K.

Fig. 3a contains two different information concerning the masses of the impinging molecules and the surface temperature. Firstly, the relative energy loss to the surface molecules increases with increasing mass of the atoms ranging from $\Delta E_{IS}/E_{inc} = 0.49$ for Ne to $\Delta E_{IS}/E_{inc} = 0.88$ for Xe at 213 K. Secondly, the data for different temperatures of the surface clearly demonstrate that the energy dissipation of gases with masses ≥ 40 amu, as shown for Ar, Kr and Xe, is not dependent on temperature and hence not affected by the thermal motion of the surface molecules. This is somewhat surprising since the condensed phase density and the liquid stiffness, as expressed by the viscosity, change substantially with the bulk phase temperature. In contrast to the heavier atoms, the energy dissipation for Ne with 20 amu shows a distinct temperature dependence; the fractional energy release increases from $\Delta E_{IS}/E_{inc} = 0.49$ at 213 K to $\Delta E_{IS}/E_{inc} = 0.64$ at 243 K.

Fig. 3b demonstrates that the probability for colliding atoms to undergo thermal equilibration on the surface and to escape with a thermal velocity distribution, as expressed by the ratio I_{TD}/I_{IS+TD}, decreases with increasing mass of the atom for both Ne and Kr. This trend, however, reverses for Xe for which we note an increase in the thermalization probability relative to Kr.

Concerning the temperature dependence it is noted that the thermalization probability, as displayed in Fig. 3b, increases with increasing temperature of the surface, independent of the colliding mass. The best fits to the temperature dependence result in the expression $0{,}005 \pm 0{,}0015 \times T$. Moreover, it is also noted that for Ne the fractional energy transfer (Fig. 3a) has the same temperature dependence as the thermalization probability (Fig. 3b). However, for colliding masses ≥ 40 amu the energy transfer is not affected by the surface temperature. This apparent contradiction will be addressed in the discussion below.

The influence on the scattering parameters as caused by the composition of the sulfuric acid–water mixture is shown in Fig. 4a and b.

This Figure contains the results for the relative energy transfer, $\Delta E_{IS}/E_{inc}$ (Fig. 4a), as well as for the probability of thermalization, $I_{TD}/(I_{IS} + I_{TD})$ (Fig. 4b), dependent on the composition of the H_2SO_4–H_2O solution. The data points for each gas include results which were averaged in steps of 1 wt% and plotted against the acid concentration between 57 and 77 wt%. The uncertainty of the reported acid concentration is within ±1 wt%.

As can be seen from the data in Fig. 4a, no significant change in the repulsive energy transfer for a change of the composition of the liquid phase is noted, with the exception of Ne and, to a smaller extent, also for Kr. This again is remarkable since the liquid stiffness of the surface, as expressed by the viscosity of the fluid, changes by almost two orders of magnitude over this concentration range. Similar observations have been made for the thermalization. In this case the fraction of colliding Ar, Kr and Xe atoms achieving thermal equilibrium is between 0.23 and 0.31 at 213 K and is not noticeably affected by the composition of the surface film. In contrast, the thermalization probability of Ne is significantly influenced by the sulfuric acid concentration on the surface. Its thermalization probability increases with increasing dilution, and hence with the probability to collide with a water molecule, from I_{TD}/I_{IS+TD} 0.6 at a sulfuric acid/water ratio of $\sim 1:1.6$ (77 wt%) to about $I_{TD}/I_{IS+TD} = 0.8$ at a ratio of $\sim 1:4.1$ (57 wt%).

5. Discussion

As demonstrated in Fig. 2a–d the observed TOF spectra and the energy distributions of the scattered atoms $P(E_{fin})$ are either single peaked or bimodal, depending on the initial translational energy. These distributions can be attributed to two limiting processes. The slow component closely follows a Maxwell–Boltzmann distribution at T_{liq} and is assigned to the trapping–desorption channel (TD). Molecules in the faster component recoil with higher translational energies and are assigned to the direct inelastic scattering channel (IS). These observations and their implications will be discussed in the following. It should be noted though that all of our results have been obtained for a fixed angle of 90° between incidence and observation. No angular dependence has been studied.

The energy distribution of the recoiled species is relatively broad and therefore the overall energy transfer onto the surface molecules is different for different atoms in the same beam. This indicates that during gas–liquid collisions the surface of the liquid does not respond like an inert, rigid wall. The inelastic energy release to the surface molecules as expressed by the $(\Delta E_{IS})/E_{inc}$ ratio increases with increasing mass of the impinging atoms. For masses ≥ 40 amu (Ar, Kr, Xe) the $(\Delta E_{IS})/E_{inc}$ values are larger than 0.5 even at high collision energies. This implies that hyper-thermal gases in contact with binary sulfuric acid/water mixtures reach thermal equilibrium at T_{liq} in only a few successive gas–liquid collisions. Even for very "hot" gases (100–200 kJ mol^{-1}) the approach to thermal velocities upon collisions with the surface appears very fast.

The observed energy transfer can be quantitatively interpreted by considering different contributions to the gas–liquid energy release. The impinging atoms can excite translational, torsional and vibrational motions of the molecules in the surface. Moreover, multiple collisions can be induced by liquid surfaces which may be considered as being rough on a molecular scale.[35,36] Such repeated collisions decelerate the translational velocity of the gas and increase their thermalization probability by deflecting it from different surface sites. The broad and bimodal energy distributions in Fig. 2d demonstrate that the recoil energies are widely distributed, indicating that there are many kinds of single and multiple collisions on a highly dynamic liquid surface.

The further analysis of our data follows the pioneering work on gas–liquid collisions performed by Nathanson *et al.*[4,30,34] and partly borrowed from studies of gas–solid collision.[31,37–43] These authors point out that gas–liquid energy transfer is dominated by the mechanical softness as well as the roughness of the surface and not by long range attractive forces during the collision. The explanation of the experimental results can therefore be provided by looking at the elementary processes of the collision dynamics on a molecular level and time scale. In the two sections below we will discuss the inelastic scattering (A) and the thermal accommodation channels (B) as a function of collision energy, impinging masses, surface temperature and acid/water composition.

A Inelastic scattering

The inelastic scattering (IS) component of a TOF spectrum corresponds to scattered atoms that do not transfer enough energy to reach thermal equilibration during the collision. For these recoiling atoms we observe that $(\Delta E_{IS}/E_{inc})$ increases with the mass of the impinging gas on sulfuric acid/water mixtures. The results obtained allow the application of the impulsive interaction model by representing the surface molecules by a single particle of mass, m_s, and by treating this surface element and the gas molecule as hard spheres in the collision.

Without intermolecular interactions the energy exchange in hard sphere collisions depends only on the mass ratio of gas

and surface atoms, $\mu = m_g/m_s$, as well as on the deflection angle. The energy transfer ($\Delta E/E_{inc}$) for a single collision between two rigid hard spheres can therefore be approximated by eqn (3):[35]

$$\frac{\Delta E}{E_{inc}} \equiv \frac{E_{inc} - E_{IS}}{E_{inc}} \approx \frac{2\mu}{(1+\mu)^2}(1 - \cos\chi(1 - \mu^2 \sin^2\chi)^{1/2} + \mu \sin^2\chi) \quad (3)$$

The attraction forces between the surface segment and the gas molecule can be approximated as a square well potential of depth V. Hence the incident particle is accelerated into the surface with energy $E_{inc} + V$.[44,45] The gas molecule then decelerates after the collision, emerging from the well with energy $E_{inc} - f(E_{inc} + V)$. In eqn (4) the intermolecular interactions have been accounted for by a factor of $(1 + V/E_{inc})$.

In addition, the thermal motions of the liquid cause the surface molecule to vibrate along the centre line. Because the relative velocity is higher when the gas and surface molecules approach each other, the net effect is to pass on momentum to the gas molecule and hence reduce energy transfer. The effect of thermal surface motion therefore decreases the energy transfer, $\Delta E/E_{inc}$, as expressed by the term $-2RT_{liq}/E_{inc}$, *viz.*

$$\frac{\Delta E}{E_{inc}} \approx \frac{2\mu}{(1+\mu)^2}(1 - \cos\chi(1 - \mu^2 \sin^2\chi)^{1/2} + \mu \sin^2\chi) \times \left[1 + \frac{V - 2RT_{liq}}{E_{inc}}\right] \quad (4)$$

Eqn (4) is a product of kinematic and energetic terms that separately control the energy transfer. The kinematic term accounts for the transfer of momentum along the centre line between the two spheres.[1]

The energy released onto the surface molecules is at a maximum when the gas approaches along the line of centres in a head-on collision and scatters directly backwards at $\chi = 180°$. In the given geometry of our experimental set up, where the observation angle for recoiling species is fixed at 90° with respect to the incident beam, $\theta_{fin} = 90° - \theta_{inc}$, the trigonometric functions can be simplified leading finally to eqn (5):

$$\frac{\Delta E}{E_{inc}} = \frac{2\mu}{(1+\mu)} \cdot \left[1 + \frac{V - 2RT_{liq}}{E_{inc}}\right] \quad (5)$$

The effects of the intermolecular forces and the thermal motions of the surface molecules on $\Delta E/E_{inc}$ decrease with increasing incident energy, E_{inc}. For hyper-thermal translational energies the momentum transfer to the surface molecules is dominated by the mass ratio $\mu = m_g/m_s$. According to eqn (5) the extent of this transfer decreases with increasing m_s and decreasing m_g.

Eqn (3)–(5) apply only to a single collision with initially stationary surface molecules. Multiple collisions, however, can occur if the incident atom strikes a patch of the surface off-centre and ricochets towards a second molecule or a different part of the same molecule. Depending on the point of contact, two or more collisions may hence be necessary for the gas molecule to escape from the surface. Impinging masses heavier than the masses of surface molecules lead to multiple collisions, since for $\mu > 1$ the incident velocity along the line-of-centres will not be reversed in a collision with an initially stationary surface molecule. Sequential collisions on a rough surface ultimately lead to a corrugation induced thermalisation since each impact further decelerates the gas molecule. The thermalization probability (TD) is also controlled by the initial trajectory of the gas molecule. When there is no barrier to adsorption, the thermalisation probability decreases as E_{inc} increases because impinging molecules with more kinetic energy are less likely to dissipate their energy fully during the initial bounces.

In the following discussion we apply the hard-sphere model to the scattering of noble gases, since eqn (3)–(5) should apply best to incoming particles that are weakly attracted to the liquids. Eqn (4) implies that intermolecular interactions on the observed energy release should only be discernible at low initial translation energies. Hence, for Ar we deduce an average well depth of only $\cong$ 3 kJ mol^{-1}, in agreement with literature data for the interaction of noble gases with other liquid surfaces.[46]

The fractional energy transfers ($\Delta E_{IS}/E_{inc}$) displayed in Fig. 3a and 4a for different impinging gases follow qualitatively the same trends as the hard sphere model, since V/E_{inc} is small at high translational energies. At $\chi = 90°$, as valid for our experimental set-up, the translational energy transfer $\Delta E_{IS}/E_{inc}$ to the surface molecules increases with increasing mass of the impinging atoms. The values ranges from $\Delta E/E_{inc} = 0.13$ for He ($m_g \sim 4$ amu) to 0.75 for Ar ($m_g \sim 40$ amu) and 0.88 for Xe ($m_g \sim 131$ amu).

The effective masses of the interacting surface segments, m_s, are calculated by converting eqn (5) into the following expression:

$$m_s = (m_g(2 - (\Delta E_{IS}))/E_{inc})/(\Delta E_{IS})/E_{inc} \quad (6)$$

This equation implies that for reverse impulsive collisions the mass of the interacting surface segment always has to exceed the mass of the impinging gas. In Fig. 5 the calculated corresponding surface masses, m_s, are displayed *versus* the masses of the colliding atoms. The values presented were calculated from the measured dependence of the energy transfer ($\Delta E_{IS}/E_{inc}$) on the mass of the colliding species, m_g.

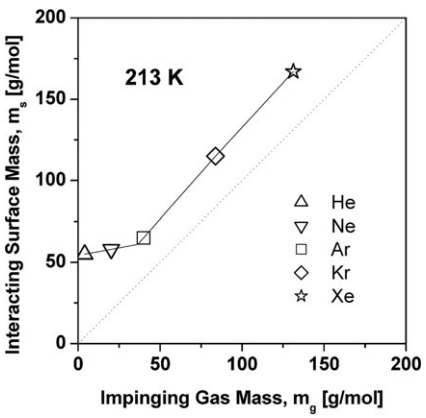

Fig. 5 Calculated effective surface mass *vs.* the mass of the impinging gas. The acid concentration is around 70 wt%.

With increasing masses of the impinging atoms the effective mass of the surface molecules participating in collisions increases from $m_s = 55$ amu for He ($m_g \cong 4$ amu) to $m_s = 167$ amu for Xe ($m_g \cong 131$ amu). The values of m_s, however, do not reflect the exact surface mass participating in collisions since eqn (6) assumes a single hard-sphere encounter only and ignores both multiple collisions and the internal structure of the liquid molecules. Especially in the case of Xe as a collider, the impinging mass ($m_{Xe} = 131$) significantly exceeds the mass of a single sulfuric acid molecule on the surface ($m_{acid} = 98$). This indicates that the reverse collision must be accomplished by multiple collisions caused by a deformation of the liquid surface.

The calculated effective mass of the interacting surface segments increase only slightly from $m_s = 55$ amu for He ($m_g = 4$ amu) to $m_s = 58$ amu for Ne atoms (amu = 20). For collision events with impinging masses ≤ 20 amu the participating surface mass corresponds roughly to the averaged molecular mass of the local surface composition ($m_s = 47$ amu, corresponding to 2 water molecules/1 sulfuric acid molecule) for the sulfuric acid–water mixture at 71.4 wt%. The experiments performed for Ne in an acid concentration range from 57 to 77 wt% indicate a decrease in the impulsive energy release to the surface with increasing sulfuric acid–water ratio (see Fig. 4a). The observed change in the energy release to the surface molecules follows the same trend as the calculated averaged molecular mass of the local surface segment as displayed in Fig. 4a. As shown in this Figure the influence of the composition diminishes with increasing mass of the impinging projectiles.

From a macroscopic point of view the stability of the scattering parameters over a wide range of compositions (57–77 wt%) are unexpected since the bulk phase parameters like bulk density, surface tension and viscosity change substantially over this concentration range. One explanation is the short contact time of impulsive collisions[47] during which distinct molecules cannot interact collectively. For instance, for particles interacting through short range repulsive forces the round trip collision time, is roughly $2d/v \cong 0.1$ ps, where $v \cong 1$ nm ps^{-1} is the gas velocity and $d \cong 0.05$ nm is the range of the inner potential well.[48] During this short time, only a small group of atoms in the liquid can respond collectively, limited by the speeds of accessible intra- and intermolecular motions. The short contact time also explains, at least in part, why the surface can change substantially in composition, liquid stiffness and transport properties but still encounters similar impulsive energy losses during collisions of gases with masses ≥ 40 amu. A useful quantity for the estimate of the transition time between a liquid's elastic response and its viscosity is given by the Maxwell relaxation time $\tau = \eta/G_\infty$, where η is the viscosity and G_∞, is the high frequency shear modulus.[49] Typical values for τ are in the range of ns and hence are substantially larger than single collision events on the 10^{-13} s timescale.

The dependence of the scattering of Ne on the acid concentration, as displayed in Fig. 4, can be explained using the kinematic model of short point contact interactions. Within this model, reverse collisions can be accounted for impinging masses ≤ 20 amu. Each of these scattering events has its own trajectory with different contributions to the experimentally observed kinematical energy release. Whereas the momentum transfer is very efficient during collision with water molecules, the fractional energy release decreases for scattering events with the heavier sulfuric acid molecules. In other words, the observed $\Delta E/E_{inc.}$ for Ne is a superposition of two different and independent scattering events, whilst the energy release to the surface strongly depends on the collision probability with either water or sulfuric acid molecules.

The opposite result, namely that the momentum transfer in the backscattering events for masses ≥ 40 amu is only weakly influenced by the amount of water molecules on the surface, may be interpreted by the fact that the impinging masses exceed the mass of the water molecules on the surface. Heavy impinging projectiles cannot be backscattered in one single collision event with a water molecule. Rather they penetrate deeper into the bulk with a changed trajectory and collide subsequently with the nearest sulfuric acid molecule.

Similar differences for Ne, in comparison with the scattering behaviour of the heavier noble gases, have also been noted for the temperature dependence as displayed in Fig. 3a. For Ne the momentum transfer to the surface molecules shows a significant increase with increasing temperature, whereas the fractional energy release for the heavier gases was nearly independent of temperature. This difference can again be explained within the kinematic model of point contact collisions. Within this model the thermal motions of the surface molecules can affect the recoil energies by changing the relative velocity between the gas atom and surface molecule, thereby altering the effective mass of the surface segments. Moreover, thermal motions change the intermolecular distances and generate gaps and protrusions that enhance the probability for sequential collisions. In hyperthermal collisions the gas-surface relative velocities should increase little with T_{liq}. The changes in relative velocity can be gauged by the effective surface mass $m_s = 58$ amu for Ne, as estimated in the previous chapter for a surface temperature of 213 K. With the assumption that the instantaneous motion of the surface fragment is directed along the line-of-contact with the Ne atom, the average increase in recoil energy due to increasing thermal motion is:

$$[\mu(2 - \mu)/(1 + \mu)^2][2RT_{liq}] \text{ where } \mu = m_g/m_s \qquad (7)$$

At 210 and 240 K the enhancements in recoil energy are 1.1 and 1.3 kJ mol^{-1}, respectively. The difference of 0.2 kJ mol^{-1} is small in comparison with the measured increase of $\Delta E/E_{inc}$ from 0.49 at 213 K to 0.65 at 243 K, which corresponds to an increase of the repulsive energy release onto the surface molecules of 12 kJ mol^{-1}. This indicates that changes of the relative velocity play a minor role in altering the recoil energies. In contrast, we expect that the density change of the liquid and the increase in surface roughness over the 30 K interval leads to a broadening of the impulsive channel for Ne, since a less dense and more coarsely packed surface promotes both sequential collisions and energy dissipation.

B Thermal desorption

Fig. 2 to 4 demonstrate that the fraction of atoms that reach thermal equilibrium during collision and subsequently desorb

from the liquid surface in a Maxwell–Boltzmann distribution equal to the surface temperature is a function of the initial translational energy, the impinging masses as well as the composition and temperature of the target. In order to discuss each of these parameters separately we have to consider that gas–liquid thermalization is controlled by several processes. The impinging gas molecule can be decelerated to low velocities by repeated impulsive collisions and can then be propelled away from the interface by thermal motions of the surface molecules. Alternatively, the gas molecule can also temporarily bind to the surface and dissolve. In addition, at collision energies approaching the vaporization energies of the liquids, the incoming particle may be able to push past one or more molecules and penetrate into the liquid before thermalisation.

It is worth noting that the analysis of the TOF spectra presented here is based on an energy determination which does not contain any information about the residence times of the gases on or in the liquid. Time resolved pulsed beam experiments performed in our laboratory[20] show that thermalized noble gases (Ar, Kr, Xe) reside on the surface of sulfuric acid water mixtures for time periods $<10^{-6}$ s, a value expected for adsorption energies of <5 kJ mol^{-1} and pre-exponential desorption factors of $\cong 10^{13}$ s^{-1}.

As can be clearly seen in Fig. 2a–d the fraction of trapping/desorption decreases as E_{inc} increases because impinging molecules with more kinetic energy are less likely to dissipate their energy fully while bouncing along the surface. Fig. 3b shows a decreasing probability of thermalization with increasing mass of the impinging projectile. The only exception is Ne. Within the point-contact model this observation can be explained by the deformation of the fluid interface. Even though the time scale of the elastic response is in the order of ns, which is very long in comparison with the 0.1-ps duration of the repulsive interaction, the incident velocity of Xe atoms cannot be reversed in a collision with an initially stationary sulfuric acid molecule. Therefore, the initial collision of the Xe atom penetrates with a changed trajectory deeper into the bulk phase.

Fig. 4b demonstrates that the thermalization of Ne atoms is significantly affected by the composition of the liquid phase, in contrast to colliding gases with masses $m_g \geq 40$ amu. A comparison of the fractional energy release (see Fig. 4a) with the thermalization probability demonstrates for Ne that the momentum transfer, $\Delta E/E_{inc}$, is accompanied with a decrease of the thermalization probability, $I_{TD}/(I_{IS} + I_{TD})$. In contrast, both probabilities are not significantly influenced by the composition of the bulk phase for the heavier gases (Ar, Kr, Xe).

Fig. 6 displays the fraction of thermalized Ne atoms as a function of the sulfuric acid concentration. This Figure also includes the normalized bulk phase ratio of water/sulfuric acid molecules on the right ordinate as derived from the bulk concentration. As can be seen, the thermalization probability decreases with increasing sulfuric acid concentration since the fractional momentum transfer of impinging Ne atoms to stationary water molecules is larger than to sulfuric acid molecules. In contrast, the thermalization probability for impinging atoms with masses ≥ 40 amu is only weakly

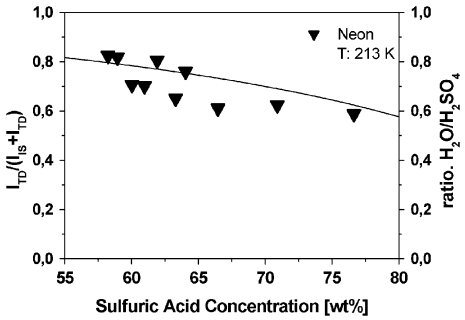

Fig. 6 Superposition of the thermalization probability, I_{TD}/I_{IS+TD}, for neon (left ordinate) and the relative ratio between water and sulfuric acid molecules (right ordinate) in dependence on the acid concentration.

affected by the surface composition. This may be interpreted by the fact that heavy projectiles cannot be thermalized in one single collision event with a water molecule, but require subsequent collisions with the nearest sulfuric acid molecule.

Fig. 4b demonstrates that the trapping desorption channel increases with increasing temperature. Over the 30-K interval the temperature dependences are linear and quite similar for all encounters. Only the temperature dependence for Ar is slightly stronger. Surprisingly, the enhanced thermalization is not accompanied by a change in the energy dissipation during collision for impinging gases with masses exceeding 40 amu.

Two possibilities for an increasing thermalization with increasing temperature, namely the thermal motions and an increasing roughness of the surface molecules, are discussed in the literature. Experiments with noble gases colliding at high energy with close-packed metal surfaces also thermalize more effectively as the temperature increases.[45,50,51] For these flat solid surfaces a roughening due to a temperature increase is not to be expected. The enhanced trapping at higher temperatures is attributed to a reduced relative velocity as some incident particles approach surface atoms and move inward towards the bulk. The effects of relative velocity should be less important in our experiments because of the high incident energies. For Ar atoms with 100 kJ mol^{-1} and interacting with a 65 amu surface mass, the impact energy decreases on average by less than 1 kJ mol^{-1} over the 30 K range for collisions with inward moving surface groups.[44] The analogous calculation for Ne atoms with initial translational energies of 85 kJ mol^{-1} implies a reduction of only 0.2 kJ mol^{-1} which is not sufficient to explain the observed change of the fractional momentum transfer of about 12 kJ mol^{-1} and the increase in the thermalization probability with temperature.

On the other hand computer simulations of fluid interfaces indicate an increasing fluctuation on the liquid surface with increasing bulk phase temperature.[2] The enhanced roughness of the phase boundary leads to an increasing probability of repeated collision. Temperature dependent experiments on the scattering of noble gases on long chain hydrocarbons indicate, in conjunction with molecular dynamic calculation, that the increasing thermalization probability is correlated with enhanced repeated collisions on the surface with increasing temperature.[2]

The role of surface temperature in affecting the physical parameters in IS/TD scattering dynamics has been investigated both experimentally and theoretically through detailed studies of the interaction of atoms with perfluorinated liquids[2] and SAM surfaces.[11,52] Such studies have shown that Ne, Ar, and Xe atoms have a greater probability to trap on a PFPE surface as the surface temperature increases.[2]

In agreement with our experimental observations such trends support a simple physical picture in which an increase in surface temperature leads to a dynamically rougher surface which promotes multiple collisions between the gas and the liquid. A surface roughening has also been correlated with the temperature dependence of bulk physical properties in case of PFPE.[53] These properties suggest that the surface of PFPE relaxes with increasing temperature into configurations where surface groups require more volume with fewer steric restrictions from neighboring groups. An increase in local surface corrugation is also coupled to an additional roughening caused by capillary waves, where random thermal oscillations increase the average thickness of the interface from 4.0 to 8.8 Å over the range of surface temperatures (232 K–323 K).[53]

6. Summary and conclusions

The repulsive energy dissipation and thermal accommodation of hyperthermal noble gas atoms colliding with a liquid sulfuric acid–water interface was studied as a function of impinging masses, translational energies as well as on the composition and the temperature of the liquid. The final energy distributions of recoiled and desorbing atoms can be attributed to two limiting processes. The slow component closely follows a Maxwell–Boltzmann distribution at T_{liq} and is assigned to thermally desorbing molecules (TD). Molecules in the faster component recoil with higher translational energies and are assigned to the direct inelastic scattering channel (IS). The dependence of the repulsive translational energy release of inelastically scattered Ne atoms on the composition of the liquid surface can be interpreted as independent collision events between Ne atoms and water as well as sulfuric acid molecules, respectively. The required energy dissipation is in agreement with theoretical assumptions that the interaction processes on the surface act collectively and occur on time scales exceeding the ps duration of a single repulsive collision.

The observed dependence of the scattering behaviour on the composition of the fluid interface decreases with increasing mass of the impinging atoms. The fractional energy release is only weakly affected by the local surface composition, indicating that the interaction of discrete surface molecules is limited by the mass ratio between impinging atoms and the molecules on the phase boundary. For backscattering, the interaction mass on the liquid surface, m_s, increases with increasing mass of the impinging projectile, m_g.

The observed increase of the thermalization probability with increasing surface temperature, independent of the colliding masses, can be qualitatively explained by increasing fluctuations on the fluid interface which promote multiple collisions. These sequential collisions enhance thermal accommodation and accelerate the approach to gas–liquid thermalization. In addition, the observed temperature dependence of the fractional energy release for Ne can also be attributed to an increasing probability of sequential collisions. In contrast, inelastic scattering of Ar, Kr and Xe is not affected by temperature.

All results obtained in this work were derived in an experimental set up in which the angles of incidents, θ_{inc}, and observations, θ_{fin}, were both fixed at 45°. Whilst the variation of θ_{inc} is not considered to be too much of concern, the inability to vary θ_{fin} is more serious. This is because the ratio of IS and TD channels might be affected by variation of the observation angles. Therefore we consider our results and their implications as being strictly appropriate only for the chosen orientation of angles. A similar argument applies to the conclusions drawn for the different noble gases because it is not entirely clear to what extent they do reflect the relative quantities of the angular distribution.

References

1 G. M. Nathanson, *Annu. Rev. Phys. Chem.*, 2004, **55**, 231–255.
2 M. E. King, M. E. Saecker and G. M. Nathanson, *J. Chem. Phys.*, 1994, **101**, 2539–2547.
3 M. E. Saecker and G. M. Nathanson, *J. Chem. Phys.*, 1993, **99**, 7056–7074.
4 M. E. Saecker and G. M. Nathanson, *J. Chem. Phys.*, 1994, **100**, 3999–4005.
5 M. E. King, G. M. Nathanson, M. A. Hanning-Lee and T. K. Minton, *Phys. Rev. Lett.*, 1993, **70**, 1026–1029.
6 T. K. Minton, M. E. King, K. M. Fiehrer and G. M. Nathanson, *J. Phys. Chem. A*, 1997, **101**, 6549–6561.
7 M. Manning, J. A. Morgan, D. J. Castro and G. M. Nathanson, *J. Chem. Phys.*, 2003, **119**, 12593–12604.
8 J. A. Morgan and G. M. Nathanson, *J. Chem. Phys.*, 2001, **114**, 1958–1961.
9 L. M. Tribe, J. A. Manning, M. D Morgan, W. R. StephensRonk, E. Treptow, G. M. Nathanson and J. Skinner, *J. Phys. Chem. B*, 1998, **102**, 206–211.
10 J. M. Zhang, D. J. Garton and T. K. Minton, *J. Chem. Phys.*, 2002, **117**, 6239; D. J. Garton, T. K. Minton, M. Alagia, N. Balucani, P. Casavecchia and G. G. Volpi, *Faraday Discuss.*, 1997, **108**, 387; D. J. Garton, T. K. Minton, M. Alagia, N. Balucani, P. Casavecchia and G. G. Volpi, *J. Chem. Phys.*, 2000, **112**, 5975; J. M. Zhang, H. P. Upadhyaya, A. L. Brunsvold and T. K. Minton, *J. Phys. Chem. B*, 2006, **110**, 12500.
11 M. E. Bennett, W. A. Alexander, J. W. Lu, D. Troya and J. R. Morris, *J. Phys. Chem. C*, 2008, **112**, 17272–17280; J. R. Lohr, B. S. Day and J. R. Morris, *J. Phys. Chem. A*, 2006, **110**, 1645; J. R. Lohr, B. S. Day and J. R. Morris, *J. Phys. Chem. B*, 2005, **109**, 15469.
12 A. J. Kenyon, A. J. McCaffery, C. M. Quintella and M. D. Zidan, *Faraday Discuss.*, 1993, **96**, 245; C. M. Quintella, A. J. McCaffery and M. D. Zidan, *Chem. Phys. Lett.*, 1993, **214**, 563; A. J. Kenyon, A. J. McCaffery, C. M. Quintella and M. D. Zidan, *J. Chem. Soc., Faraday Trans.*, 1993, **89**, 3877; A. J. Kenyon, A. J. McCaffery, C. M. Quintella and M. D. Zidan, *Chem. Phys. Lett.*, 1992, **190**, 55.
13 S. P. K. Kohler, M. Allan, H. Kelso, D. A. Henderson and K. G. McKendrick, *J. Chem. Phys.*, 2005, **122**, 024712; H. Kelso, S. P. K. Kohler, D. A. Henderson and K. G. McKendrick, *J. Chem. Phys.*, 2003, **119**, 9985; F. Ausfelder, H. Kelso and K. G. McKendrick, *Phys. Chem. Chem. Phys.*, 2002, **4**, 473; M. Allan, P. A. J. Bagot, S. P. K. Kohler, S. K. Reed, R. E. Westacott, M. L. Costen and K. G. McKendrick, *Phys. Scr.*, 2007, **76**, C42; M. Allan, P. A. J. Bagot, R. E. Westacott, M. L. Costen and K. G. McKendrick, *J. Phys. Chem. C*, 2008, **112**, 1524; M. Allan, P. A. J. Bagot, M. L. Costen and K. G. McKendrick, *J. Phys. Chem. C*, 2007, **111**, 14833; S. P. K. Kohler, S. K. Reed, R. E. Westacott and

K. G. McKendrick, *J. Phys. Chem. B*, 2006, **110**, 11717; S. P. K. Kohler, M. Allan, M. L. Costen and K. G. McKendrick, *J. Phys. Chem. B*, 2006, **110**, 2771.
14 B. G. Perkins, T. Haber and D. J. Nesbitt, *J. Phys. Chem.*, 2005, **A109**, 16396; B. G. Perkins and D. J. Nesbitt, *J. Phys. Chem.*, 2006, **110**, 17126; B. G. Perkins and D. J. Nesbitt, *J. Phys. Chem.*, 2007, **111**, 7420.
15 S. A. Vazquez, J. R. Morris, A. Rahaman, O. A. Mazyar, G. Vayner, S. V. Addepalli, W. L. Hase and E. Martinez-Nunez, *J. Phys. Chem.*, 2007, **A111**, 12785; T. Y. Yan, N. Isa, K. D. Gibson, S. J. Sibener and W. L. Hase, *J. Phys. Chem.*, 2003, **107**, 10600; T. Y. Yan, W. L. Hase and J. R. Barker, *Chem. Phys. Lett.*, 2000, **329**, 84; T. Y. Yan and W. L. Hase, *Phys. Chem. Chem. Phys.*, 2000, **2**, 901.
16 G. Li, S. B. M. Bosio and W. L. Hase, *J. Mol. Struct.*, 2000, **556**, 43.
17 D. Kim and G. C. Schatz, *J. Phys. Chem. A*, 2007, **111**, 5019.
18 R. Zellner, in *Topics in Physical Chemistry*, ed. H. Baumgärtel, W. Grünbein and F. Hensel, Guest Editor R. Zellner, Steinkopff/ Springer, Darmstadt, 1999, vol. 6, pp. 181–247.
19 B. J. Finlayson-Pitts and J. N. Pitts, *Chemistry of the Upper and Lower Atmosphere*, Academic Press, New York, 2000.
20 P. Behr, U. Scharfenort and R. Zellner, *Phys. Chem. Chem. Phys.*, submitted.
21 C. Radüge, V. Pflumio and Y. R. Shen, *Chem. Phys. Lett.*, 1997, **274**, 140–144.
22 S. Baldelli, C. Schnitzer, J. M. Shultz and D. J. Campbell, *Chem. Phys. Lett.*, 1998, **287**, 143–147.
23 C. Schnitzer, S. Baldelli and M. J. Shultz, *Chem. Phys. Lett.*, 1999, **313**, 416–420.
24 D. H. Fairbrother, H. Johnston and G. Somorjai, *J. Phys. Chem.*, 1996, **100**, 13696–13700.
25 H. Chen and D. E. Irish, *J. Phys. Chem.*, 1971, **75**, 2672–2681.
26 T. F. Young and G. E. Walrafen, *Trans. Faraday Soc.*, 1961, **57**, 34–39.
27 K. S. Carslaw, S. L. Clegg and P. Brimblecombe, *J. Phys. Chem.*, 1995, **99**, 11557–11574.
28 L. R. Williams and F. S. Long, *J. Phys. Chem.*, 1995, **99**, 3748–3751.
29 S. L. Lednovich and J. B. Fenn, *AIChE J.*, 1977, **23**, 454–459.
30 G. M. Nathanson, *Annu. Rev. Phys. Chem.*, 2004, **55**, 231–255.
31 C. T. Rettner, E. K. Schweizer and C. B. Mullins, *J. Chem. Phys.*, 1989, **90**, 3800–3813.
32 D. J. Auerbach, G. Comsa, B. Poelsema, M. Asscher and G. Sormorjai, in *Atomic and Molecular Beam Methods*, ed. G. Stoles, Oxford University, New York, 1988 and 1992, vols. I and II.
33 J. E. Hurst, C. A. Becker, J. P. Cowin, K. C. Janda, L. Wharton and D. J. Auerbach, *Phys. Rev. Lett.*, 1979, **43**, 1175–1177.
34 M. E. Saecker, S. T. Govoni, D. V. Kowalski, M. E. King and G. M. Nathanson, *Science*, 1991, **252**, 1421–1424.
35 N. Lipkin, R. Gerber, N. Moiseyev and G. M. Nathanson, *J. Chem. Phys.*, 1994, **100**, 8408–8417.
36 R. B. Gerber, A. T. Yinnon, M. Yanuka and D. Chase, *Surf. Sci.*, 1992, **272**, 81–93.
37 J. A. Barker and D. J. Auerbach, *Surf. Sci.*, 1985, **4**, 1–99.
38 S. R. Cohen, R. Naaman and J. Sagiv, *Phys. Rev. Lett.*, 1987, **58**, 1208–1211.
39 S. R. Cohen, R. Naaman and J. Sagiv, *J. Chem. Phys.*, 1988, **88**, 2757–2763.
40 Y. Paz and R. Naaman, *J. Chem. Phys.*, 1991, **94**, 4921–4927.
41 J. Harris and W. H. Weinberg, in *Dynamics of Gas Surface Interactions*, ed. C. T. Rettner and M. N. R. Ashfold, Royal Society of Chemistry, Cambridge, 1991.
42 M. Logan, in *Solid State Surface Science*, ed. M. Green, Marcel Dekker, New York, 1973, vol. 3, pp. 1–103, ch. 1.
43 F. O. Goodman and H. Y. Wachman, *Dynamics of Gas-Surface Scattering*, Academic, New York, 1976.
44 E. K. Grimmelmann, J. C. Tully and M. J. Cardillo, *J. Chem. Phys.*, 1980, **72**, 1039–1043.
45 J. R. Barker and D. J. Auerbach, *Faraday Discuss. Chem. Soc.*, 1985, **80**, 277–289.
46 I. Benjamin, M. Wilson and and A. J. Pohorille, *Chem. Phys.*, 1994, **100**, 6500.
47 A. Gelb, B. G. Sumpter and D. W. Noid, *J. Phys. Chem.*, 1990, **94**, 809–814.
48 J. Harris, *Phys. Scr.*, 1987, **36**, 156–165.
49 G. Harrison, *The Dynamic Properties of Supercooled Liquids*, Academic, New York, 1976.
50 R. M. Logan and R. E. Stickney, *J. Chem. Phys.*, 1966, **44**, 195–201.
51 C. T. Rettner, C. B. Mullins, D. S. Bethune, D. J. Auerbach, E. K. Schweizer and W. H. Weinberg, *J. Vac. Sci. Technol., A*, 1990, **8**, 2699–2704.
52 N. Isa, K. D. Gibson, T. Yan, W. Hase and S. J. Sibener, *J. Chem. Phys.*, 2004, **120**, 2417–2433.
53 B. G. Perkins, T. Haber and D. J. Nesbitt, *J. Phys. Chem.*, 2008, **B112**, 507–519.

